COMPUTATIONAL ASSISTED DEVELOPMENT OF HIGH TEMPERATURE STRUCTURAL MATERIALS

R. K. Kalia,* P. Vashishta,* R. Benedek,[1,2] C. Woodward,[1,3] S. I. Rao,[1,3] and D. M. Dimiduk[3]
*Louisiana State University, Baton Rouge, LA 70803
[1]UES Inc., Dayton, OH 45432
[2]Northwestern University, Evanston, IL 60208
[3]Air Force Research Lab., Wright Patterson AFB, OH 45433-6533

Abstract

Major aeronautical and space programs are clearly paced by the status of emerging high temperature materials. These Grand Challenge simulations are designed to give insight into material design problems for ceramic and metallic systems. In the past year, we have made a great deal of progress in understanding properties and processes in ceramic materials using parallel molecular dynamics (MD) simulations based on realistic interatomic interactions. Research achievements in this area include:

- Study of sintering, structure, and mechanical behavior of nanophase SiC, Si_3N_4, and SiO_2;
- 10-million atom nanoindentation simulation of crystalline Si_3N_4 and dynamic fracture in nanophase Si_3N_4;
- 30 - 100 million atom MD simulations of dynamic fracture;
- Investigation of dynamics of oxidation of Al nanoclusters using a variable-charge MD simulation approach which explicitly includes dynamic charge transfer between Al and O;
- Determination of residual stresses in Si/Si_3N_4 nanopixels using 10 million atom MD simulations.

Highly efficient load-balancing and data compression algorithms as well as multiresolution schemes to evaluate interatomic interactions were developed to perform large-scale MD simulations on massively parallel machines.

In the metallic systems we have made significant progress in modeling metal-oxide interfaces using parallel-scalable first principles methods based on the density functional theory. The misfit dislocation network and interface morphology were determined for a model {222}MgO/Cu polar interface using a 400 atom simulation cell. Relaxation of the atomic layers on both sides of the interface is characterized.

Structure and Mechanical Properties of Nanophase SiC and SiO_2

Advanced structural ceramics are highly desirable materials for applications requiring extreme operating conditions. Light weight, elevated melting temperatures, high strengths, and wear and corrosion resistance make them very attractive for high-temperature and high-stresses applications. The only serious drawback of ceramics is that they are brittle at low to moderately high temperatures.

In recent years a great deal of progress has been made in the synthesis of ceramics that are much more ductile than conventional coarse-grained materials (Pechenik, Kalia, and Vashishta, 1999). These so called nanophase materials are fabricated by in-situ consolidation of nanometer size clusters. Despite a great deal of research, many perplexing questions concerning nanophase ceramics remain unanswered. Experiments have yet to provide information regarding the morphology of pores or the structure and dynamics of atoms in nanophase ceramics. As far as modeling is concerned, only a few atomistic simulations of nanophase materials have been reported thus far. This is due to the fact that these simulations are computationally very demanding: A realistic simulation of a

nanophase solid requires 10^5-10^6 time steps for processing and ~ 10^6 atoms since each nanocluster itself consists of 10^3-10^4 atoms.

Molecular dynamics simulations have been performed to investigate the structure and mechanical behavior of nanophase SiC and SiO_2. Interatomic potentials in these simulations consist of two- and three-body terms. The two-body terms are steric repulsion and screened Coulomb potentials due to charge transfer between atoms, and a charge-dipole interaction that takes into account the large electronic polarizability of anions. The three-body terms take into account covalent effects through bond-bending and bond-stretching terms. These interatomic interactions are validated by comparing the MD results with a variety of experimental measurements. We find: i) bond lengths and bond-angle distributions in crystalline systems are in excellent agreement with experiments; ii) positions and relative heights of various peaks in the static structure factor for amorphous Si_3N_4, SiC, and SiO_2 are in good agreement with neutron scattering measurements; iii) phonon densities-of-states of crystalline and amorphous systems agree well with inelastic neutron scattering experiments; and iv) elastic moduli of crystalline and amorphous systems are also in good agreement with experimental values.

Recently we performed the first joint experimental and MD study of nanophase SiC (n-SiC). Both experiment (open circles in Fig. 1) and simulations (solid diamonds in Fig. 1) reveal the onset of sintering around 1500K. The MD simulations provide a microscopic picture of how the morphology of micropores in n-SiC changes with pressure. The fractal dimension and the surface roughness exponent of micropores are found to be 2.4 and 0.45, respectively, over the entire pressure range between 0 and 15 GPa. Small-angle neutron scattering at low wavevectors yields a fractal dimension of 2 for pores in n-SiC. MD calculations of pair-correlation functions and bond-angle distributions reveal that interfacial regions between nanoparticles are highly disordered with nearly the same number of 3-fold and 4-fold coordinated Si atoms. Atomic diffusivities of Si and C in inter-particle regions are considerably larger than those inside the particles. The effect of consolidation on mechanical properties is also investigated with the MD approach. The results show a power-law dependence of elastic moduli on the density with an exponent of 3.4 ± 0.1.

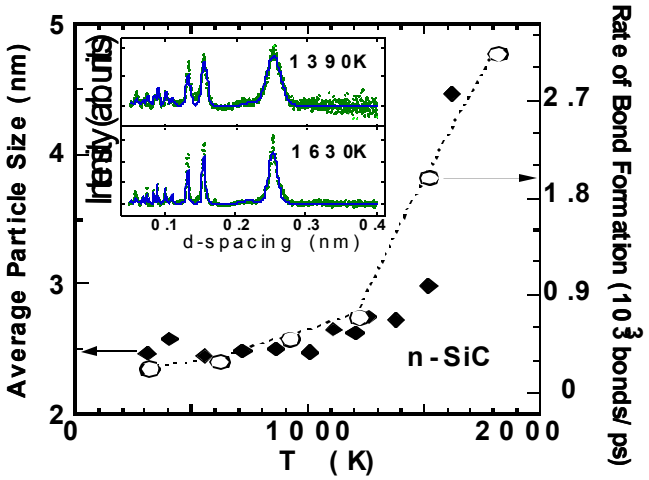

Fig. 1: The onset of sintering is indicated by the increase in the average particle size in the neutron data (◆) and the increase in the rate of bond formation between nanoparticles in the MD results (o). The dotted line is a guide to the eye for the MD results. The inset shows the observed powder-diffraction pattern (dots) and the fits (lines) to the crystalline *b*-SiC structure.

The investigation of nanophase SiO_2 involves amorphous nanoclusters which were obtained from bulk amorphous SiO_2. By sintering at different pressures, we generated nanophase solids with densities ranging from 76% to 93% of the bulk amorphous density (2.2 g/cm^3). In these solids the morphology of micropores, mechanical behavior, and the effect of nanoscale structures on the short-range and intermediate-range order (SRO and IRO) are investigated. Pores in nanophase a-SiO_2 are found to have a self-similar structure with a fractal dimension close to 2 and the pore surface width scales with the volume as, $W \sim \sqrt{V}$. The MD simulations reveal that the SRO in nanophase silica glass is very similar to that in the bulk glass: both of them consist of corner-sharing $Si(O_{1/2})_4$ tetrahedra.

However, the IRO in nanophase silica glass is quite different from that in the bulk glass (Campbell et al., 1999). In the nanophase silica glasses the first sharp diffraction peak (FSDP), the signature of IRO, has a much smaller height and is shifted to smaller wavevectors relative to the FSDP in the bulk silica glass, see Fig. 2. From the partial static structure factors and pair distribution functions, we find that Si-O and Si-Si correlations in the range of 4 – 10 Å are primarily responsible for differences in the IRO of bulk and nanophase silica glasses. We have also investigated the mechanical behavior of nanophase a-SiO_2. The elastic moduli are found to have a power law dependence on the density with an exponent of 3.5. These results are in excellent agreement with experimental measurements on high-density silica aerogels.

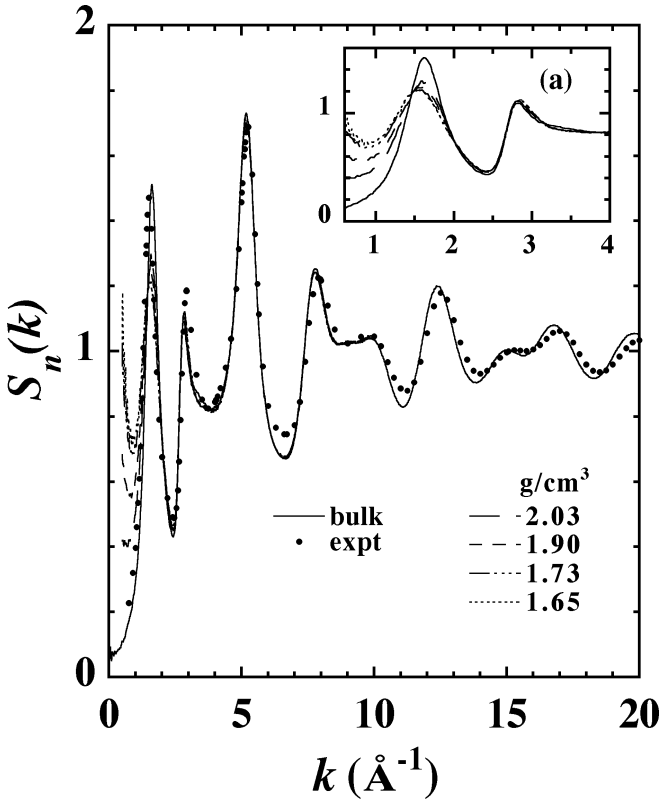

Fig. 2: Neutron-scattering static structure factor, $S_n(k)$, for bulk and nanophase a-SiO_2. Solid and dashed lines, MD results; solid dots, neutron-diffraction experiments for bulk a-SiO_2 [P. A. V. Johnson *et al.*, J. of Non-Cryst. Solids **58**, 109 (1983)]. Inset (a): magnification of the FSDP region.

Nanoindentation in Si_3N_4

Using multimillion atom MD simulations we are investigating nanoindentation in silicon nitride (Walsh et al., 1998). Nanoindentation testing is a unique local probe of mechanical properties of materials. This technique is especially useful in testing surfaces and thin films. The importance of atomistic-level understanding of indentation processes is widely recognized. Recent progress in parallel computing and multiscale algorithms allows unprecedented realism in atomistic simulations of indentation.

The nanoindentation simulation is performed on a 600Å × 600Å × 300Å crystalline α-Si_3N_4 slab consisting of 10 million atoms (see Fig. 3). The sample is indented using a pyramid indentor with a load ~ 10 μN and indentation depth ~ 100Å. These values are within the resolution of nanoindentation experiments. Having established the methodology for atomistic simulation of nanoindentation, this virtual nanohardness approach is being used to probe high-temperature properties where actual indentation measurements may not be possible.

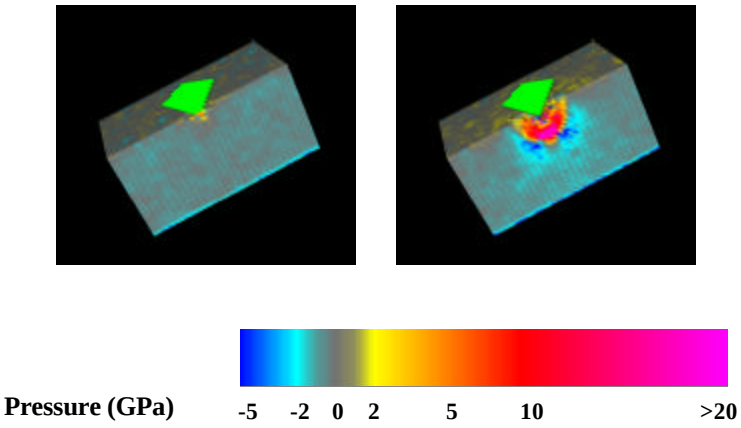

Fig. 3: A half-slice view of the silicon nitride sample before and after the nanoindentation simulation at 300 K. Local amorphization near the indentor results in residual stresses.

Dynamic Fracture in Silicon Carbide and Gallium Arsenide: 30 - 100 Million Atom MD Simulations

Recently we investigated dynamic fracture in crystalline β-SiC at various temperatures using large-scale MD simulations. The simulation sample is a SiC strip of 30 million atoms. After inserting a notch, we relax the system at 0K with the conjugate gradient approach. Subsequently, the system is heated gradually to 300K and then a constant strain is applied in the *x* direction by displacing atoms in the *y*-*z* plane that are within 5Å from the boundaries of the system. For this strip geometry, the mechanical energy release rate, G, of the system can be calculated from the knowledge of the applied strain, ε, and the value of the stress, σ, far ahead of the crack tip: $G = W\sigma\varepsilon/2$, where W is the width of the strip. In addition to the mechanical energy release rate, we monitor the crack-tip velocity and local stress distribution at various temperatures. At high temperatures, we find the onset of fracture occurs at a much larger value of G because of dissipative effects such as dislocations, micropore formation and coalescence, and crack deflection. In contrast, fracture at room temperature is cleavage-like with hardly any dissipation. Figure 4 shows fracture for three different orientations of the notched surface: i) in the case of (110) surface, the fracture is cleavage like; ii) for (111), dislocations are emitted during crack propagation; and iii) for (001), crack branching is observed.

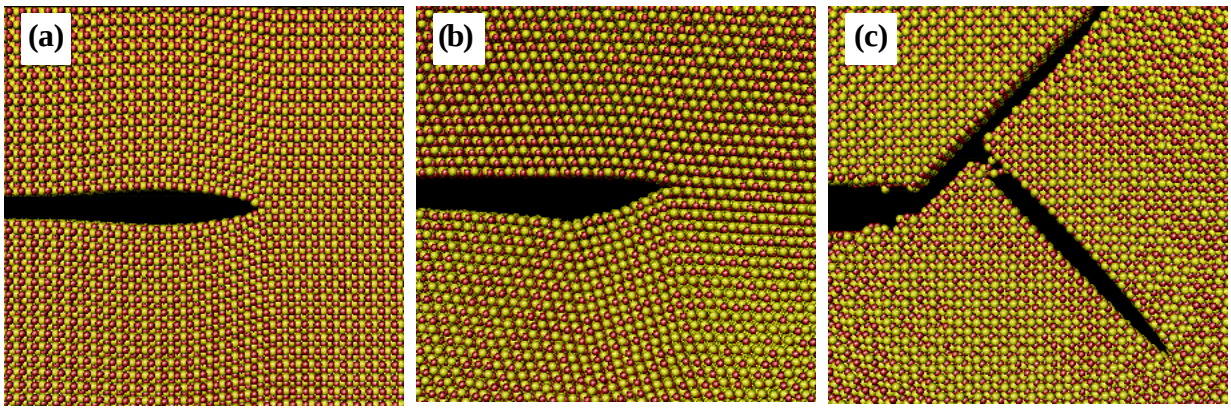

Fig. 4: Fracture of SiC for (a) (110), (b) (111), and (c) (001) surfaces.

Recently we have also investigated dynamic fracture in crystalline GaAs using 100 million atom MD simulations. The main focus of this work is the brittle-to-ductile transition in GaAs. Preliminary results indicate that the transition occurs around 600K. This is close to the experimental value for the brittle-to-ductile transition temperature (630 - 660K).

Dynamics of Oxidation of Aluminum Nanoclusters

In recent times, consolidated solids composed of nanometer size clusters (nanophase materials) have drawn a great deal of attention because of their unique thermo-mechanical, electrical, and magnetic properties. A particularly interesting possibility is the synthesis of nanostructured composites consisting of metallic nanoclusters coated with a passivation layer. Upon compaction, the passivation layer forms a boundary layer between the isolated metallic grains. The presence of the passivating network is known to have a dramatic effect on the electrical, chemical, and mechanical behavior of the material. In a recent study by Sánchez-López et al. (1996), Al/Al-oxide nanocomposites were found to have a metallic shine and an ohmic electrical resistivity that was dependent upon the compaction conditions. The nanocomposite consisted of 300 Å aluminum particles with an interconnected 40 Å oxide layer that prevented the material from falling apart when heated to temperatures above the melting point of aluminum. Other studies point out that the properties of these nanocomposite materials are strongly dependent on the nature of the passivation layer.

We have performed the first successful MD simulation of the oxidation of an Al-nanocluster (diameter 200 Å). Structural and dynamic correlations in the oxide region and the evolution of various quantities including charge, surface oxide thickness, diffusivities of atoms, and local stresses have been calculated (Campbell et al., 1999). The MD simulations are based on a highly reliable interaction scheme developed by Streitz and Mintmire (1994) that can successfully describe a wide range of physical properties of Al and Al_2O_3. This scheme is capable of treating: i) both metallic and ceramic systems; ii) bond formation and bond breakage; and iii) changes in charge transfer as the atoms move and their local environments are constantly altered. Dynamic charge transfer gives rise to a computationally intensive Coulomb interaction which, for the number of atoms necessary in a realistic simulation, requires highly efficient algorithms that map well onto parallel architectures. We have implemented the fast multipole method (FMM) of Greengard and Rokhlin (1987) for the long-range Coulomb interaction (this reduces the computational complexity from $O(N^2)$ to O(N)) with extensions for stress calculations, and the multiple time-step algorithm of Tuckerman et al. (1992, this can further reduce the execution time by an order of magnitude). Both algorithms are well suited for parallel architectures.

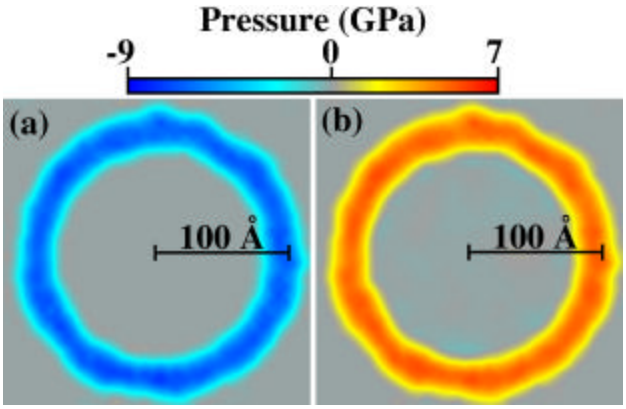

Fig. 5: (a) Electrostatic and (b) non-electrostatic contributions to the local pressure in the nanocluster after 100 ps of simulation time.

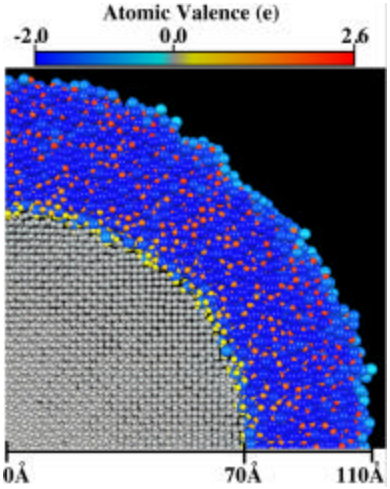

Fig. 6: Snapshot of a small slice (115 Å × 115 Å × 8 Å) of the Al nanocluster after 466 ps of simulation time. The larger spheres correspond to oxygen and smaller spheres to aluminum; color represents the sign and magnitude of the charge on an atom.

The MD simulation for the oxidation of an Al nanocluster reveals large negative pressure contribution from electrostatic forces due to charge transfer is partially offset by the positive contribution of the steric repulsion in the oxide region, see Fig. 5. This results in the oxide remaining largely under negative pressure, which causes aluminum

to diffuse towards the surface and oxygen to diffuse towards the interior of the cluster. Structural analysis reveals that a 40 Å thick amorphous oxide scale consisting of mixed octahedral, $Al(O_{1/6})_6$, and tetrahedral, $Al(O_{1/4})_4$, configurations is formed during 466 ps of simulation time, see Fig. 6. This is in excellent agreement with experimental results on aluminum nanoclusters. The average mass density in the oxide scale is 75% of the crystalline alumina density. Owing to variations in aluminum and oxygen densities, structures in the oxide scale vary when passing through the oxide from the metal-oxide interface to the oxide-environment interface.

Residual Stresses in $Si/Si/Si_3N_4$ Nanopixels: 10 Million Atom MD Simulations

We have performed a 10 million atom parallel molecular dynamics simulation of atomic-level stress distribution in a $Si/Si/Si_3N_4$ nanopixel (Bachlechner et al., 1998). The system consists of a 539Å×32Å×10Å Si mesa which is placed on top of a 1077Å×653Å×300Å Si(111) substrate. Periodic boundary conditions are used in the plane of the substrate. The bottom layer of Si atoms in the substrate is fixed to the bulk Si lattice constant to simulate the effect of an infinite substrate. The top surface of the mesa is covered with an 83Å-thick crystalline (Fig. 7(a)) or amorphous (Fig. 7(b)) $Si_3N_4(0001)$ film. The $Si(111)/c\text{-}Si_3N_4(0001)$ interface involves a 1.1% lattice mismatch inducing a stress in the system. The lattice mismatch causes compressive stresses in Si_3N_4, while a tensile stress is observed in Si (Fig. 7(a)). Note the effects of surfaces and edges on the stress. In the case an $a\text{-}Si_3N_4$ film, we find the stress to be non-uniform laterally, as seen in Fig. 7(b), which is quite different from that for crystalline films. Lateral stress domains on the scale of 300Å are observed in the case of amorphous Si_3N_4 film. As the PECVD films employed are polycrystalline, such a lateral inhomogeneity in stress is expected in the films employed and our results reveal a hitherto unappreciated serious consideration for the processing of nanoscale pixels.

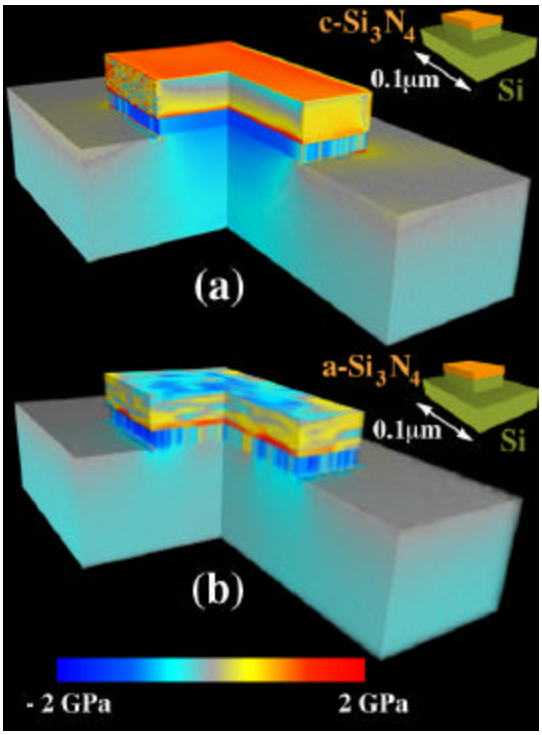

Fig. 7: (a) Stress distribution in a $Si/Si/Si_3N_4$ nanopixel in the presence of lattice mismatch. (b) Stress distributions in a nanopixel covered with amorphous silicon nitride. To show the stresses inside the nanopixel, one quarter of the system is removed and the value of the hydrostatic stress is color coded.

First Principles Calculations of the Atomic Structure of Ceramic/Metal Interfaces

High temperature structural metals are often used in an oxidizing environment and the integrity of these components is dependent on the presence of a stable oxide scale. Understanding and controlling the evolution of these interfaces over the use lifetime of a component is a critical alloy design problem for emerging alloy systems and the materials currently in service. For example, while the refractory metal intermetallics have been shown to have superior strength and creep properties for temperatures in excess of 1000°C, controlling oxidation rates of these materials remains a serious alloy design problem. Also, the use lifetime of the so-called "Nickel-based super-alloys" in turbine engines is limited by the failure of ceramic thermal barrier coatings.

The complexity of the chemical bonding at ceramic-metal interfaces, which incorporate aspects of ionic, covalent, metallic and van der Waals interactions, has been an obstacle to performing realistic simulations of their atomic structure. First-principles calculations within the density functional theory framework appear the most promising approach to improve our understanding of these systems, although they are highly computationally intensive. We have applied such calculations to simulate {222}MgO/Cu, a model ceramic metal interface which has been extensively studied experimentally, particularly by electron microscopy, and atom-probe field-ion microscopy. Two significant features of {222}MgO/Cu are its polarity (the atomic layers on the oxide side are either purely anion or purely cation; experimentally, the terminating layer at the interface is invariably found to be oxygen) and the large lattice-constant mismatch, which results in a closely-spaced misfit-dislocation network (every 6 atoms on the MgO side, and every seven atoms on the Cu side) at the interface. Previous first-principles calculations for ceramic-metal interfaces have neglected the lattice-constant misfit; its inclusion in the present work make this one of the largest first-principles calculations performed to date. The periodic unit cell comprises four layers of O, three layers of Mg, and three layers of Cu arranged in a slab. Initially all 399 atoms are in perfect lattice positions. In each step of the calculation, the self-consistent electronic structure is determined, from which the (Hellmann-Feynman) forces on the atoms are obtained. The atoms are then relaxed towards equilibrium and the cycle is repeated until the atomic forces are essentially zero. In some previous phenomenological analyses of the structure of this interface, only the Cu atoms were assumed to relax from their perfect lattice sites. The results of our first principles calculations show that both oxygen and copper atoms at the interface undergo significant relaxation as a result of interactions across the interface. Figure 8 depicts the mean atomic layer coordinate normal to the interface, *z*, on the abscissa, and the layer buckling, represented by the standard deviation of this coordinate for a given layer, on the ordinate. The buckling of the oxygen layer at the interface is smaller that that of the interface copper layer but is not negligible.

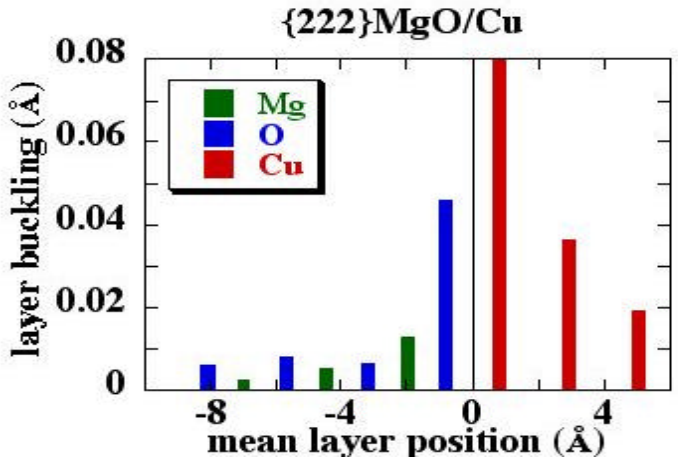

Fig. 8: Layer buckling, as measured by the standard deviation of the coordinate normal to the interface plane, versus the position of the layer relative to the interface plane.

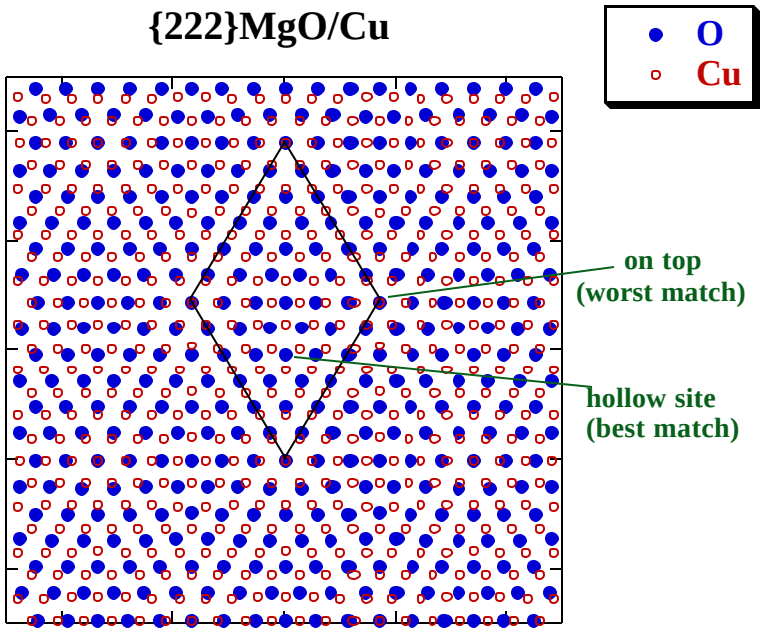

Fig 9: Atomic coordinates of the Cu and O interface layers projected onto the plane of the interface. The network of misfit dislocations connects nodes of worst match, at which O and Cu atoms are directly opposite each other.

The layer unit cell of the calculation, outlined in Figure 9, is repeated periodically. The figure may be interpreted as a periodic array of regions of good match (near the centers of the two triangles that make up the unit cell) interspersed with regions of poor match (at the corners). Misfit dislocation lines connect the points of worst match. Figure 10 illustrates the distortion of atomic rows in the <211> directions within the interface layers. Rows of Cu and O atoms that are straight in the perfect crystals become curved with a periodicity consistent with the spacing of the dislocation network.

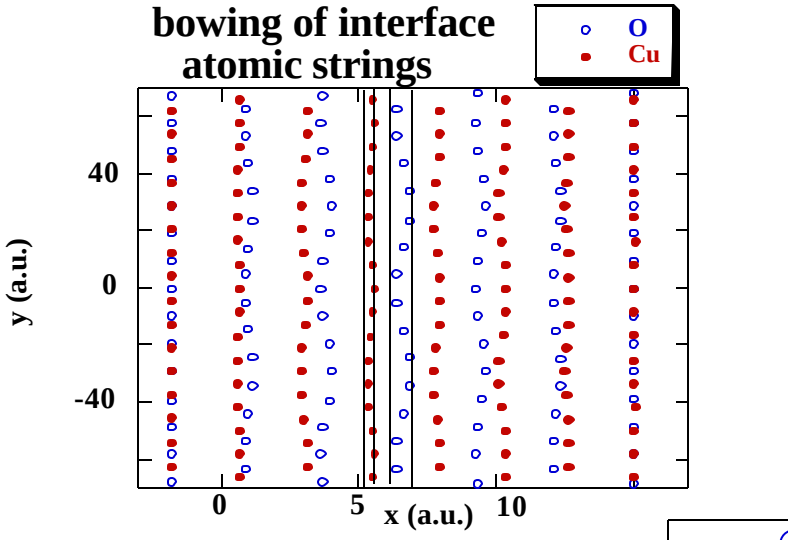

Fig. 10: Rows of atoms in <211> directions within the Cu and O interface layers. Note the abscissa scale has been expanded in order to accentuate the bowing of the atomic rows.

These calculations represent an extremely large-scale application of first principles methods to determine the atomic structure of a ceramic-metal interface including lattice misfit. This is a necessary step towards developing a detailed understanding of the influence of atomic structure and the controlling role of impurities on interface adhesion. The following are a few technical details regarding the calculations. We have employed the parallel pseudopotential plane wave program FEMD (A. Alavi et al. 1994). FEMD is based on a preconditioned Krylov-space iterative Lanczos-method diagonalization procedure, and is an extension by the Queen's University Belfast group of earlier Car-Parrinello codes developed at the IBM Ruschlikon Laboratory. Although multi-hundred-atom first principles calculations have been done previously, they were primarily restricted to materials like Si where a relatively small basis set is adequate. Treating systems of this size that involve first row and transition elements is a significant challenge and was made possible only by exploiting parallelism, as well as by using highly optimized kinetic energy filtered pseudopotentials with a cutoff of only 47 Ry. The real space mesh is 108x108x108, and the 1300 electron orbitals are expanded in approximately 90,000 plane waves. Memory requirements dictated running on 128 processors. Achieving self consistency for the starting configuration required about 6000 proc.-hrs, and reoptimizing the orbitals after an atomic relaxation step required 2-3000 proc.-hrs. Since dozens of relaxation steps are needed to relax the atoms to equilibrium, the full calculation requires of the order 100,000 proc.-hrs.

Acknowledgments

This work is supported by AFOSR through Grant Nos. F 49620-94-1-0444 and F 33615-96-C-5258, the U.S. Department of Energy, through Basic Energy Sciences Grant No. DE FG02-96ER45597 and a subcontract No. B346019 (MSD). Computations have been performed at Naval Oceanographic Office (NAVO), Aeronautical Systems Center (ASC), Corps of Engineers Waterways Experiment Station (CEWES), and the Concurrent Computing Laboratory for Materials Simulations at LSU.

References

1. A. Pechenik, R. K. Kalia, and P. Vashishta, *Computer-Aided Design of High-Temperature Materials* (Oxford Univ. Press, Oxford, 1998).
2. T. Campbell, R. K. Kalia, A. Nakano, F. Shimojo, K. Tsuruta, and P. Vashishta, Phys. Rev. Lett., in press.
3. J. C. Sánchez-López *et al*., NanoStruct. Mater. **7**, 813 (1996).
4. F. H. Streitz and J. W. Mintmire, Phys. Rev. B **50**, 11996 (1994).
5. L. Greengard and V. Rokhlin, J. Comp. Phys. **73**, 325 (1987).
6. M. Tuckerman *et al*., J. Chem. Phys. **97**, 1990 (1992).
7. M. E. Bachlechner, A. Omeltchenko, A. Nakano, R. K. Kalia, P. Vashishta, I. Ebbsjö, A. Madhukar, and P. Messina, Appl. Phys. Lett. **72**, 1969 (1998).
8. A. Alavi, J. Kohaniff, M. Parrinello, and D. Frenkel, Phys. Rev. Lett. **73**, 2599 (1994).